

Long range energy transfer in conjugated polymer sequential bilayers

L. A. Cury, K. N. Bourdakos, DeChang Dai, F. B. Dias, and A. P. Monkman

Citation: *J. Chem. Phys.* **134**, 104903 (2011); doi: 10.1063/1.3560164

View online: <http://dx.doi.org/10.1063/1.3560164>

View Table of Contents: <http://jcp.aip.org/resource/1/JCPSA6/v134/i10>

Published by the [American Institute of Physics](#).

Additional information on *J. Chem. Phys.*

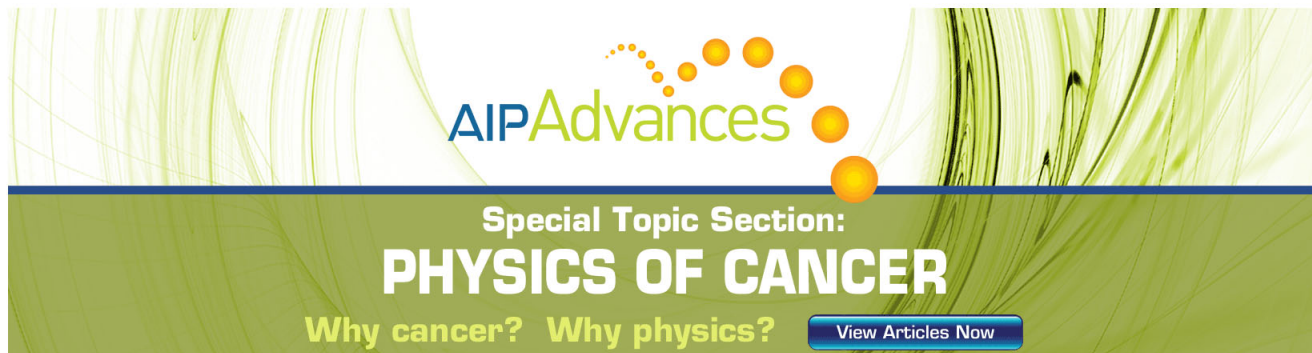
Journal Homepage: <http://jcp.aip.org/>

Journal Information: http://jcp.aip.org/about/about_the_journal

Top downloads: http://jcp.aip.org/features/most_downloaded

Information for Authors: <http://jcp.aip.org/authors>

ADVERTISEMENT



AIPAdvances

Special Topic Section:
PHYSICS OF CANCER

Why cancer? Why physics? [View Articles Now](#)

Long range energy transfer in conjugated polymer sequential bilayers

L. A. Cury,^{1,a)} K. N. Bourdakos,^{2,a)} DeChang Dai,² F. B. Dias,² and A. P. Monkman²¹*Departamento de Física, Instituto de Ciências Exatas, Universidade Federal de Minas Gerais, 31270-901 Belo Horizonte, Minas Gerais, Brazil*²*Department of Physics, University of Durham, South Road, Durham DH1 3LE, United Kingdom*

(Received 23 September 2010; accepted 8 February 2011; published online 10 March 2011)

Steady-state and time-resolved photoluminescence have been used to investigate the optical properties of bilayer and blend films made from poly(9,9-dioctyl-fluorene-2,7-diyl) (PFO) and poly[2-methoxy-5-(2-ethylhexyloxy)-1,4-phenylenevinylene] (MEH PPV). Energy transfer has been observed in both systems. From steady-state photoluminescence measurements, the energy transfer was characterized by the effective enhancement of the MEH PPV emission intensity after exciting the donor states. Relatively faster decays for the PFO donor emission have been observed in the blends as well as in the bilayer structures, confirming effective energy transfer in both structures. In contrast to the bilayers, the time decay of the acceptor emission in the blends presents a long decay component, which was assigned to the exciplex formation in these samples. For the blends the acceptor emission is in fact a composition of exciplex and MEH PPV emissions, the later being due to Förster energy transfer from PFO. In the bilayers, the exciplex is not observed and temperature dependence photoluminescence measurements show that exciton migration has no significant contribution to the energy transfer. The efficiency and very long range of the energy transfer in the bilayers is explained assuming a surface–surface interaction geometry where the donor/acceptor distances involved are much longer than the common Förster radius. © 2011 American Institute of Physics. [doi:10.1063/1.3560164]

I. INTRODUCTION

One of the advantages in working with luminescent polymers, beyond their optical properties, applicability and relatively low costs of production, is the simple and practical technique for fabricating solid thin films. Certainly, one of the most popular techniques is the spin-coating technique. Although there are some limitations to the spin-coating technique regarding the fabrication of multilayer structures or even simple bilayers, which proved to be of interest, mainly for polymeric light emitting device (PLED) applications. Those difficulties have been often overcome by using a combination of orthogonal solvents and film annealing steps. From the point of view of the transport properties, a bilayer structure composed by *p*- and *n*-type polymers can provide a better match to the anode and cathode work functions, respectively, in order to reach a balanced injection of both carriers which improves the PLED electroluminescence (EL) efficiency.^{1–3} Bilayer structures also make possible the fabrication of PLEDs where the tunability of the EL wavelength was observed as a function of the applied voltage.⁴ New features in the EL spectra not directly accessible from the ground state of the constituent polymers have been observed and ascribed to the exciplex emission at the bilayer interface.⁵ Exciton diffusion is another issue that has been explored using bilayer structures. Roughly speaking, excitons created by illumination can reach the bilayer interface and

undergo interfacial charge separation with direct application to photovoltaic structures.⁶ In addition, the poly[2-methoxy-5-(2-ethylhexyloxy)-1,4-phenylenevinylene] (MEH PPV) photoluminescence quantum yield (PLQY) in the bilayer structure is shown to increase at least 4% in comparison to the previous PLQY in the literature⁷ due to the energy transfer efficiency. This could be explored in PLED devices to enhance the EL of MEH PPV or another acceptor polymer.

The component layers in the bilayer structure were prepared by sequential spin-coating process. Thin enough layers were fabricated in order to minimize self-absorption effects but thicker ones were also fabricated for the sake of comparison and confirmation of the bilayer structure formation. Even though some mixing occurs at the bilayer interface due to the action of the solvent of the second layer, this will not compromise the structure that can still be useful to probe the interfacial interplay of excitons in such films.⁸ This intermixing region at the bilayer interface, however, could result in a kind of material possessing the same characteristics of a blend. The poly(9,9-dioctyl-fluorene-2,7-diyl) (PFO):MEH PPV blends were also made by spin-coating at different concentrations of the MEH PPV acceptor. In fact, some equivalent properties in blends and bilayers have been observed, however, significant differences between them have been achieved by the analysis of the respective time-resolved photoluminescence decays. Thus, the aim of this work will be focused on the comparison of the optical properties of real blend and bilayer films and how the energy transfer is affected by the different structures.

^{a)} Authors to whom correspondence should be addressed. Electronic mail: cury@fisica.ufmg.br and k.n.bourdakos@durham.ac.uk.

II. SAMPLES AND EXPERIMENTAL DETAILS

Blend solutions of PFO and MEH PPV were produced at different concentrations of MEH PPV, corresponding respectively to 1.0%, 5.4%, and 11.5% by weight to 10mg of PFO. All the blend solutions were dissolved in 5.0 ml of ρ -xylene and preheated in a water bath at 80 °C for 10 min before leaving to stir for more than 12 h. Blended films were fabricated by spin-coating on glass substrates at 1000 rpm. The thickness of the blend at 5.4%, measured by ellipsometry in a J. A. Woollan Co., Inc. ellipsometer, model M2000, was $L_{\text{Blend}} = (12 \pm 1)$ nm, which was considered a representative thickness for all the blends since their solutions have similar concentrations ($C \approx 2.0$ mg/ml).

For the thinnest bilayer B1, we first spread a 2.2 mg/ml solution of MEH PPV in ρ -xylene at 1000 rpm on top of a glass substrate. The MEH PPV film was heated at 80 °C in a hot plate, for 30 min, to further remove the solvent. A hexamethyldisilane (HMDS) solution was deposited by spin-coating at 1000 rpm on top of the MEH PPV film prior to the PFO deposition in order to promote its better spreading. The HMDS coated surface becomes neutral, hydrophobic, and nonoily. In addition, it offers increased resistivity and is not affected by solvents that are not readily hydrolyzed. The bilayer structure was completed by spreading a 5.0 mg/ml solution of PFO in toluene at 2000 rpm. It was heated again at 80 °C in a hot plate during 30 min to further remove the toluene. The spreading of the PFO solution on top of the MEH PPV film must be done between 5 and 7 s before spinning in order to minimize the time of contact. The total thickness of the bilayer B1 was $L_{\text{B1}} = (34 \pm 2)$ nm. From a model considering the MEH PPV and PFO adjacent layers on top of the glass substrate we were able to fit the ellipsometric data, with the respective layer thickness given by $L_{\text{B1-MEH}} = (19 \pm 1)$ nm and $L_{\text{B1-PFO}} = (15 \pm 1)$ nm. The pure PFO film was also fabricated by spin-coating on a glass substrate at 2000 rpm from a 5.0mg/ml toluene solution.

The standard photoluminescence (steady-state) and absorption measurements were performed, respectively, in a Jobin Yvon Horiba Fluorolog fluorimeter and in a Shimadzu model UV3600 spectrophotometer at room temperature and in the air. The PLQY measurements were performed using a polytetrafluoroethylene-coated integrating sphere (Lab Sphere) mounted into the fluorimeter.⁹ Time-resolved photoluminescence decays were collected using the picosecond time correlated single photon counting technique (instrument response function 24 ps, 76 MHz repetition rate). The films were excited by a second harmonic pulse ($\lambda = 393$ nm) from a mode-locked Ti:sapphire laser from Coherent Inc., with vertical polarization. The emission was detected through a double-subtractive monochromator (SpectraPro-2300i), and a MCP detector (Hamamatsu model R3809U-50) was used to collect decays at 424 nm and at 565 nm.

III. RESULTS AND DISCUSSIONS

The pure PFO, the PFO:MEH PPV blends, and the PFO/MEH PPV bilayers were characterized by absorption, photoluminescence (PL), and time-resolved photolumines-

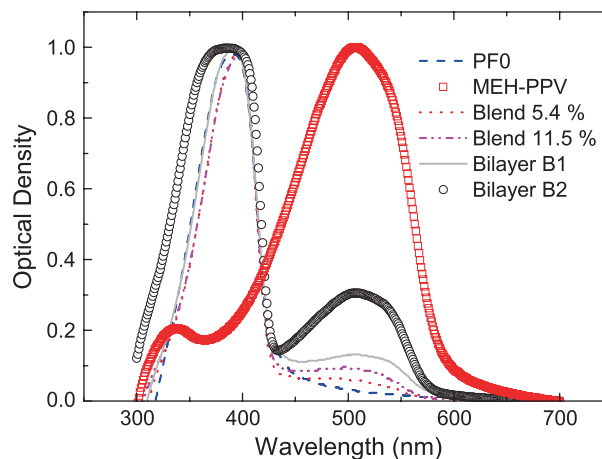


FIG. 1. Absorption spectra for the pure PFO film, for the pure MEH PPV film, for the films at 5.4% and 11.5% concentration of MEH PPV in the blend, and for the thinnest bilayer B1. The open circles spectrum corresponds to the bilayer B2 where the PFO and MEH PPV layers were, respectively, made by spin-coating at 800 rpm from a 10 ml/mg toluene solution and at 1000 rpm from a 4.4 ml/mg ρ -xylene solution. The MEH PPV absorption spectra were measured using a film done with the same parameters as the MEH PPV layer in the bilayer B2. The spectra were normalized for comparison.

cence in air at room temperature. The absorption spectra are shown in Fig. 1, where they are normalized for better comparison. The blends present a relatively small optical density in the MEH PPV absorption region (wavelengths higher than 430 nm), while for the bilayers it increases due to the relatively higher amount of acceptor used. However, from the absorption spectra we can clearly distinguish between thicker (B2) and thinner (B1) bilayers. The sequence of layers for the thickest bilayer B2 is described in the caption of Fig. 1.

The PL spectra for the blends, the bilayer B1, and for the pure PFO and MEH PPV films are shown in Fig. 2(a). All the films were excited at 373 nm, which corresponds to a wavelength around the maximum absorption of the PFO and the relatively small absorption for the MEH PPV (Fig. 1). Other bilayers beyond B1 and B2 have been fabricated. The energy transfer effect has been observed in all the bilayers. The bilayer emission intensity is though dependent on the direction of excitation, which is not the case for the blends. However, when thin enough component layers are made, the emission intensity becomes practically the same, independent of the excitation direction, as has been observed for the thinner bilayer B1. In this paper only the results with the excitation through the PFO side are presented.

As a way to compare the energy transfer efficiencies for bilayers and blends, we have used the ratio between the MEH PPV peak intensity at two different excitation wavelengths. Excitation at 373 nm, the situation where the energy transfer from PFO to MEH PPV actually occurs and direct MEH PPV excitation is minimal, and excitation at 488 nm, the wavelength at which only the MEH PPV can be excited. In a pure MEH PPV film (PL spectrum shown in Fig. 2) the PL peak intensity I_{373} for the excitation at 373 nm is smaller than the PL peak intensity I_{488} for the excitation at 488 nm due to the relatively higher absorption at 488 nm (see Fig. 1). The ratio between them is 0.489. For the blends and bilayers, however,

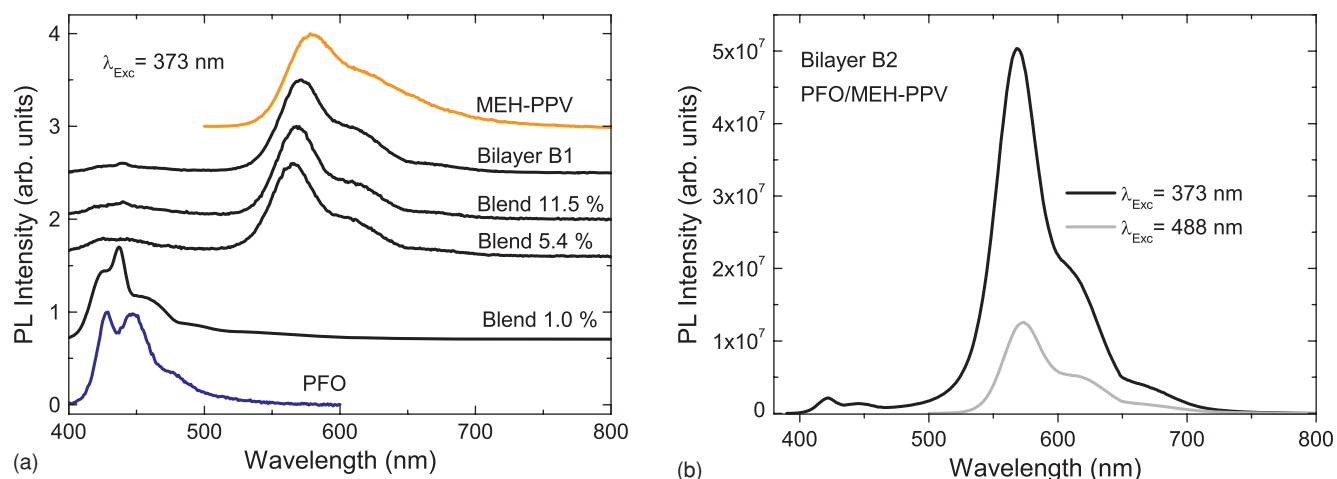


FIG. 2. (a) PL spectra acquired at an excitation wavelength of 373 nm for the PFO and MEH PPV single films, for the blends and for the bilayer B1. The spectra were normalized and displaced for clarity. In real terms the emission of the MEH PPV single film is at least one order of magnitude smaller than the emission in blends and bilayers. (b) The PL spectra for the thickest bilayer B2. The black line spectrum was acquired with a wavelength excitation at 373 nm at which the MEH PPV has a poor absorption. The gray line spectrum corresponds to the MEH PPV emission with the bilayer being excited at 488 nm, at which the absorption of the PFO almost vanishes.

the acceptor peak intensity I_{373} for the excitation at 373 nm becomes larger than the I_{488} because the energy transfer contribution from the PFO to the MEH PPV sites takes place. The ratio I_{373}/I_{488} reaches values of 11.8, 10.1, and 7.2, respectively, for the blends at 5.4% and 11.5% MEH PPV concentrations, and for the thinnest bilayer B1. Figure 2(b) shows the representative spectra obtained for the thickest bilayer B2 at 373 and 488 nm excitation wavelengths, with a smaller ratio $I_{373}/I_{488} = 3.5$.

The PLQY was also calculated for the blends at 5.4% and 11.5% MEH PPV concentrations and for the thinner bilayer B1. The values considering to just the MEH PPV integrated intensity were, respectively, $(19 \pm 1)\%$, $(17 \pm 1)\%$, and $(14 \pm 1)\%$, which are comparable to the value of $(21 \pm 2)\%$ obtained for the pure PFO film and follow the same trend of the ratios discussed above. Taking into account the PLQY and the values of the ratios discussed above, we can conclude that both the thinnest bilayer and the blends present comparable energy transfer performances. It is not expected that bilayers and blends behave in the same way since in the bilayers the dominant excited region of the donor can be far apart from the acceptor. This statement is in agreement with the smallest ratio obtained for the bilayer B2, that possess the thicker PFO donor layer.

The effective enhancement of the PL intensity for the MEH PPV emission followed by the strong decrease of the PFO PL intensity due to energy transfer was not observed for the blend film at 1.0%, as shown in Fig. 3. The excitation of this film at 488 nm only yields a very small MEH PPV emission that needs to be multiplied by 20 times in order to be barely compared to the tail of the spectrum obtained at 373 nm.

The PL decays acquired at 424 nm for the blends and for the bilayer B1, corresponding to the PFO emission region and their best fits, are shown in Fig. 4. In Fig. 5 are shown the acceptor decays for the blends and for the bilayer B1 at a collection wavelength of 565 nm. All fitting curves are

sums of two or three exponentials. The fitting parameters with insignificant weight and without clear physical content have been omitted, as their physical interpretation was beyond the scope of this work and their omission does not compromise our analysis and conclusions. A global analysis involving simultaneously the data acquired at 424 nm and at 565 nm have also been performed, confirming the general trends of the data in Table I. In the same table the average lifetimes calculated by the expression $\bar{\tau} = \sum (I_i \tau_i^2) / \sum I_i \tau_i$ were included (we have considered all fitting parameters in these calculations). This makes much easier to compare the different decays and to perceive the effect of the MEH PPV layer in the bilayer structure and of the increase of the MEH PPV amount in the blends.

The PL decay intensity at 424 nm (Fig. 4) for the blend at 1.0% can be well fitted with a triple exponential function

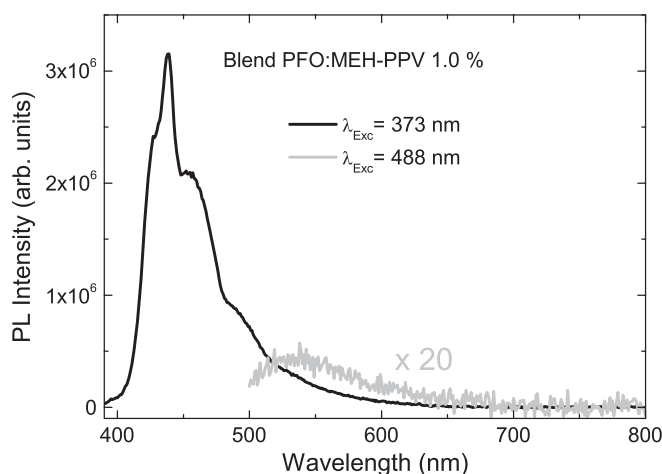


FIG. 3. PL spectra for the 1.0% concentration of MEH PPV in the blend. The black and grey line spectra were acquired, respectively, at 373 nm and 488 nm excitation wavelengths. The gray line was multiplied by 20 in order to show the faint emission of the MEH PPV.

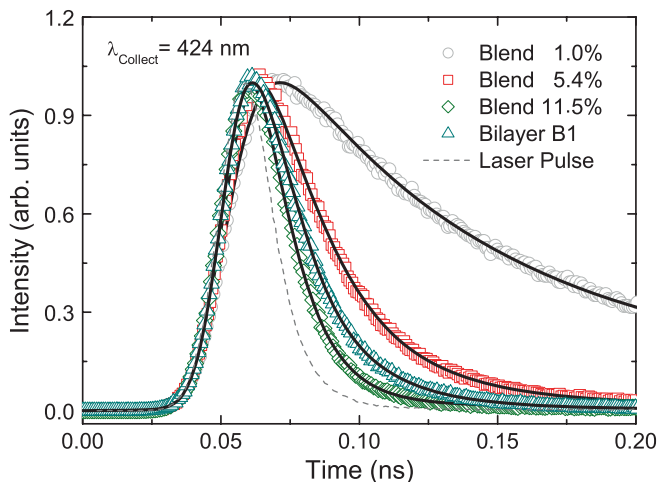


FIG. 4. Normalized photoluminescence decays acquired at 424 nm, corresponding to the PFO emission region for the thinner bilayer (open triangles) and for the blends at 1.0% (open circles), 5.4% (open squares), and 11.5% (open diamonds) MEH PPV concentrations. The black full lines are the best fits of the decays as discussed in the text. The dashed line corresponds to the excitation laser pulse at 393 nm.

($I(t) = \sum_{i=1}^3 I_{li} e^{-t/\tau_{li}}$), with the parameters I_{li} and τ_{li} (see Table I for a comparison) close to those obtained for the pure PFO decay (not shown in Fig. 4 for the sake of clarity). This similarity would be expected since energy transfer has not been observed in this case. The two faster lifetime components of 48 and 135 ps for the blend at 1.0% are interpreted as the result of intramolecular and/or intermolecular redistribution energy mechanisms due to exciton migration and energy traps before the final PFO radiative state recombination corresponding to the longer decay at 380 ps.¹⁰ Faster decays τ_{l1} and τ_{l2} , however, are observed for the bilayer and for the blends at 5.4% and 11.5% MEH PPV concentrations, which is a consequence of the effective energy transfer rate to the MEH PPV sites.

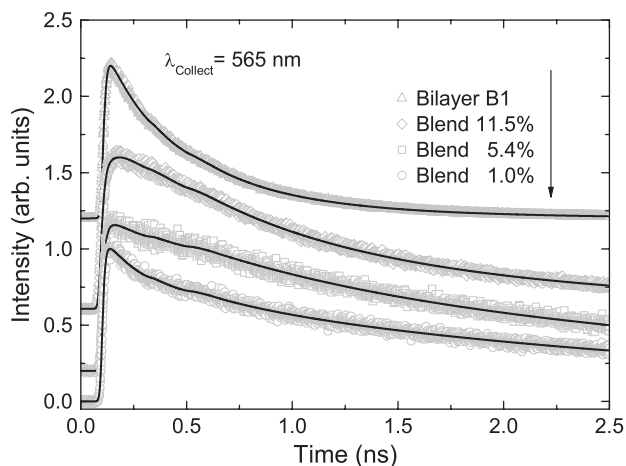


FIG. 5. Normalized photoluminescence decays acquired at 565 nm, corresponding to the MEH PPV emission region for the bilayer B1 (open triangles) and for the blends at 1.0% (open circles), 5.4% (open squares), and 11.5% (open diamonds) MEH PPV concentrations. The black full lines are the best fits of the decays as discussed in the text. The decays were displaced for more clarity.

TABLE I. Main fitting parameters and average lifetimes of pure PFO, of blends at 1.0%, 5.4%, and 11.5% MEH PPV concentrations and of the bilayer B1.

Pure PFO film ($\lambda_{\text{Collect}} = 424 \text{ nm}$)			
$I_1 = 0.501$	$\tau_1 = 43 \text{ ps}$		
$I_2 = 0.478$	$\tau_2 = 137 \text{ ps}$		
$I_3 = 0.021$	$\tau_3 = 385 \text{ ps}$		
$\bar{\tau} = 137 \text{ ps}$			
Blend PFO:MEH PPV 1.0%			
$\lambda_{\text{Collect}} = 424 \text{ nm}$		$\lambda_{\text{Collect}} = 565 \text{ nm}$	
$I_{l1} = 0.44$	$\tau_{l1} = 48 \text{ ps}$	$I_{r1} = 0.367$	$\tau_{r1} = 252 \text{ ps}$
$I_{l2} = 0.54$	$\tau_{l2} = 135 \text{ ps}$	$I_{r2} = 0.633$	$\tau_{r2} = 2933 \text{ ps}$
$I_{l3} = 0.02$	$\tau_{l3} = 380 \text{ ps}$		
$\bar{\tau} = 135 \text{ ps}$		$\bar{\tau} = 2806 \text{ ps}$	
Blend PFO:MEH PPV 5.4%			
$\lambda_{\text{Collect}} = 424 \text{ nm}$		$\lambda_{\text{Collect}} = 565 \text{ nm}$	
$I_{l1} = 0.907$	$\tau_{l1} = 20 \text{ ps}$	$I_{r1} = 0.19$	$\tau_{r1} = 550 \text{ ps}$
$I_{l2} = 0.093$	$\tau_{l2} = 61 \text{ ps}$	$I_{r2} = 0.81$	$\tau_{r2} = 2159 \text{ ps}$
$\bar{\tau} = 86 \text{ ps}$		$\bar{\tau} = 2068 \text{ ps}$	
Blend PFO:MEH PPV 11.5%			
$\lambda_{\text{Collect}} = 424 \text{ nm}$		$\lambda_{\text{Collect}} = 565 \text{ nm}$	
$I_{l1} = 0.9844$	$\tau_{l1} = 10 \text{ ps}$	$I_{r1} = 0.518$	$\tau_{r1} = 750 \text{ ps}$
$I_{l2} = 0.0156$	$\tau_{l2} = 60 \text{ ps}$	$I_{r2} = 0.166$	$\tau_{r2} = 2418 \text{ ps}$
$\bar{\tau} = 26 \text{ ps}$		$\bar{\tau} = 1616 \text{ ps}$	
Bilayer B1			
$\lambda_{\text{Collect}} = 424 \text{ nm}$		$\lambda_{\text{Collect}} = 565 \text{ nm}$	
$I_{l1} = 0.88$	$\tau_{l1} = 5.6 \text{ ps}$	$I_{r1} = 0.68$	$\tau_{r1} = 277 \text{ ps}$
$I_{l2} = 0.12$	$\tau_{l2} = 27 \text{ ps}$	$I_{r2} = 0.32$	$\tau_{r2} = 683 \text{ ps}$
$\bar{\tau} = 14 \text{ ps}$		$\bar{\tau} = 495 \text{ ps}$	

The consecutive increase of τ_{r1} for the blends is interpreted as a more complex MEH PPV recombination probably due to intermediary intermolecular MEH PPV/PFO complexation states (steric interactions) that would take place with increasing MEH PPV concentration in the blend. The acceptor decay for all blends present a long tail behavior, with a decay component τ_{r2} , which is not observed in the bilayer (see Fig. 5 and Table I). These long components can not be related to the formation of the MEH PPV domains in the PFO matrix. Shorter PL lifetime of 200 ps has been measured for the MEH PPV in a blend with polyethylene (PE).¹¹ This lifetime is inside the range of 200–500 ps reported for the MEH PPV in solution,^{11–13} in solid state film and in a MEH PPV/PE gel.¹¹

The energy levels, highest occupied (HOMO) and lowest unoccupied (LUMO) molecular orbitals, for the PFO and for the MEH PPV are, respectively, $\text{HOMO}_{\text{PFO}} = -5.8 \text{ eV}$, $\text{LUMO}_{\text{PFO}} = -2.85 \text{ eV}$ (Ref. 14) and $\text{HOMO}_{\text{MEH}} = -5.1 \text{ eV}$, $\text{LUMO}_{\text{MEH}} = -2.7 \text{ eV}$.¹⁵ The offset between the HOMO and LUMO levels strongly suggest the possibility of exciplex formation between PFO and MEH PPV. Such exciplex emission in the blends would take place around 551 nm in the region where the acceptor decays have been collected. We assigned the long decay component in the acceptor emission decay to the presence of the exciplex.^{16,17}

In the bilayers, the MEH PPV peak emission occurs in the range of 570 to 573 nm. The exciplex formation in this case is expected only in the intermixing interface region between the PFO and the MEH PPV layers and it would not contribute effectively to MEH PPV emission. The annealing

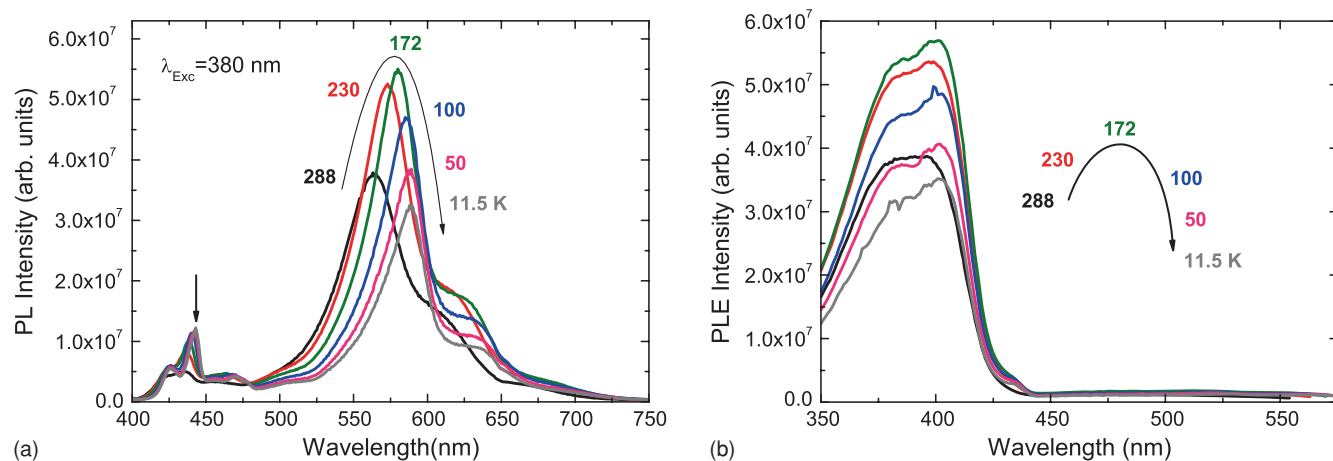


FIG. 6. (a) Photoluminescence spectra at different temperatures for the blend at 5.4% of MEH PPV concentration. The excitation wavelength for all the spectra was $\lambda_{\text{Exc}} = 380$ nm. (b) The corresponding photoluminescence excitation spectra at the same temperatures as in (a). The value of the collect wavelength (λ_{Collect}) at each PLE spectrum has been varied corresponding to the respective position of the MEH PPV emission peak.

process of the polymer layer or the use of the HMDS during the fabrication of the bilayers do not affect the MEH PPV or the PFO emissions. The possible explanation for the difference in the peak emission of the pure MEH PPV [$\lambda_p = 580$ nm, Fig. 2(a)] is that in the pure MEH PPV film, the self-absorption redshifts the emission. The observed redshifts of MEH PPV peaks in the bilayers for the excitation at 488 nm compared to the MEH PPV peak positions when excited at 373 nm favors this assumption. For the blends at 5.4% and 11.5% MEH PPV concentrations, the MEH PPV peak emissions appear, respectively, at $\lambda_p = 557.0$ nm and $\lambda_p = 560.0$ nm. These small blueshifts compared to the MEH PPV peak positions in the bilayers can be interpreted as being due to the overlap of the exciplex and the MEH PPV emissions. In addition, in a blended film the MEH PPV domains inside the PFO matrix could not present the same conformational structure of the molecules as in a MEH PPV film. A relatively smaller average conjugation length can

take place by bends, molecular crosslinks, and different pack conditions.

In the blends, the exciplex formation must occur due to excitations at the PFO/MEH PPV interfaces. Furthermore, this could be enhanced by the migration of a PFO exciton to a site where molecules of MEH PPV are in the range of the exciton dissociation length. Förster energy transfer to a MEH PPV site will also contribute to the total PL emission of the acceptor. In order to characterize the occurrence of the exciton migration in the bilayers and blends we have performed PL and photoluminescence excitation (PLE) measurements at different temperatures. In Figs. 6(a) and 6(b), and Figs. 7(a) and 7(b) are shown, respectively, the PL and PLE spectra for the blend at 5.4% of MEH PPV concentration and for a bilayer B3, the structure of which is described in the caption of Fig. 7. The exciton migration is a thermally activated process.¹⁸ The exciplex formation also requires some thermal energy to drive the formation. Thus, at lower temperatures the

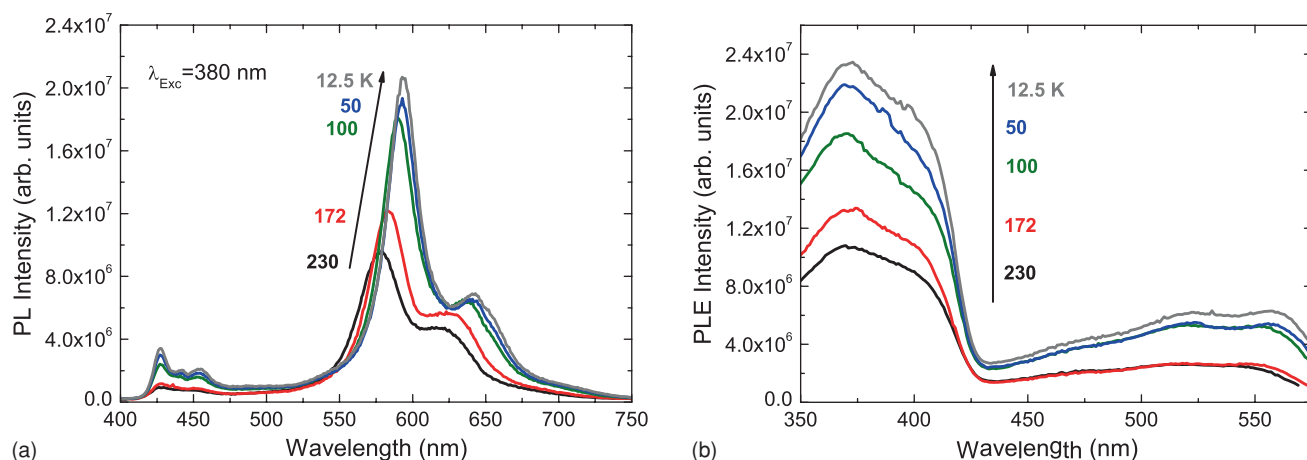


FIG. 7. (a) Photoluminescence spectra at different temperatures for the bilayer B3 where the PFO and MEH PPV layers were, respectively, made by spin-coating at 2000 rpm from a 10 ml/mg toluene solution and at 2000 rpm from a 4.4 ml/mg *p*-xylene solution. The excitation wavelength for all the spectra was $\lambda_{\text{Exc}} = 380$ nm. The total thickness of the bilayer B3 was $L_{B3} = (144 \pm 4)$ nm, with $L_{B3-\text{MEH}} = (26 \pm 1)$ nm and $L_{B3-\text{PFO}} = (118 \pm 3)$ nm. (b) The corresponding photoluminescence excitation spectra at the same temperatures as in (a). The value of the collect wavelength (λ_{Collect}) at each PLE spectrum has been varied corresponding to the respective position of the MEH PPV emission peak.

exciton migration and the exciplex emission intensity tend to decrease.

In the case of the blend, a sharp increase in the PL intensity occurs when the sample is cooled at room temperature down to 172 K [Fig. 6(a)]. However, a clear drop in the intensity is observed when the sample is cooled down to 100 K with a further reduction when the temperature cooling down to 50 K and finally to 11.5 K. The PLE spectra follow the same trend [Fig. 6(b)]. The decrease of the acceptor PL intensity at low temperatures indicates that exciton migration occurs in the blends. Although exciton migration can still occur at low temperatures it is relatively reduced. The remaining PL intensity observed at 11.5 K [Fig. 6(a)] is more likely due to MEH PPV emission induced by Förster energy transfer mechanism. The arrow in Fig. 6(a) indicates the PFO β -phase peak intensity, which appears due to the cooling temperature effect.^{19,20}

For the bilayer (see Table I) the lifetime term τ_{r1} is assigned as the recombination lifetime of the MEH PPV acceptor. The value of 277 ps for the MEH PPV at room temperature is in agreement with other results in the literature^{11,21} although this lifetime can depend on the average conjugation length of the polymer. The term $\tau_{r2} = 683$ ps is interpreted as a recombination of more complex MEH PPV mixing states at the interface of the bilayer. In contrast to the blends, the decay of the bilayer B1 has no long lifetime component. The relatively longer emission decays observed for the acceptor states in the blends imply that the donor/acceptor interaction in bilayers and blends do not have the same origin. In addition, the PL and PLE intensities for the bilayer [Fig. 7(a) and 7(b)] monotonically increase with decreasing temperature. In these bilayer films the Förster energy transfer dominates.

As in the blend films, the MEH PPV emission itself redshifts with decreasing temperature, but as can be seen when comparing Figs. 6(a) and 7(a), the broadening of the PL acceptor spectrum to the lower wavelength side in the bilayer is lower than in the blend, which correspond to a very little contribution from exciplex emission. The full width at half maximum of the acceptor PL spectra at room temperature are 53 nm and 47 nm, respectively, for the blend and for the bilayer.

The contribution of $\tau_{r1} = 277$ ps lifetime term indicates that energy transfer occurs between PFO and MEH PPV sites, which are far away from the bilayer interface. In the recent past, a long range interaction has been described in poly(*N*-vinylcarbazole) and poly(9,9'-di-*n*-hexyl-2,7-fluorenylvinylene) bilayer systems due to energy migration.²² In our case the energy transfer in the bilayers is qualitatively explained, as described below, considering a long range interaction based on a surface-surface geometry. This means that PFO \leftrightarrow MEH PPV energy transfer in the bilayers can occur at larger distances compared to the Förster radius²³ or to the exciton dissociation length.

The Förster radius R_0 , defined as the donor/acceptor separation distance for which direct donor decay is equally likely to transfer energy to the acceptor, has been calculated from the expression,²⁴

$$R_0 = 0.211 \left\{ k^2 \eta_D n^{-4} \left[\int_0^\infty f_D(\lambda) \epsilon_A(\lambda) \lambda^4 d\lambda \right] \right\}^{1/6}, \quad (1)$$

where k^2 is an orientation factor equal to 2/3 for randomly oriented dipoles, $\eta_D = 0.21$ is the measured donor PLQY, $n = 1.9$ is the refractive index²⁵ of the medium, $f_D(\lambda)$ is the PL spectrum of the donor normalized by area, and $\epsilon_A(\lambda)$ is the molar extinction coefficient of the acceptor, which was obtained based on the measured acceptor absorbance and the ϵ_A at 488 nm measured in Ref. 26. The Förster radius was calculated to be $R_0 = (4.6 \pm 0.3)$ nm. The error in R_0 accounts the assumption that the acceptor chromophores could be formed by 8–15 monomer units.

The Förster radius of 4.6 nm, can explain the energy transfer achieved in the blends with the average donor-acceptor separation R predicted by the energy transfer rate,²⁴

$$k_{ET} = \frac{1}{\tau_0} \left(\frac{R_0}{R} \right)^6, \quad (2)$$

where τ_0 is the donor radiative lifetime. However, the Förster dipole-dipole interaction theory cannot explain the results achieved for the bilayers. The intensity of the excitation light drops exponentially across the 100 nm PFO layer, therefore, the PFO emission is dominated by the first 20 nm of the thicker donor layer. Thus, the exciton would have to migrate a distance much larger than exciton dissociation length (~ 10 nm)¹⁹ to explain the observed PFO \leftrightarrow MEH PPV energy transfer in these structures. A more appropriate description should take into account a surface-surface interaction in the bilayers with the energy transfer rate $k_{ET} \propto R^{-2}$, as has been observed experimentally in Refs. 27–29.

Considering that in the blends and in the bilayer the PFO emission was almost completely quenched [Fig. 2(a)], the PFO lifetime is practically equal (Fig. 4), and the performance energy transfer ratios as calculated above are of the same order of magnitude, we can roughly estimate the donor/acceptor separation in the bilayer by considering the energy transfer rates of blends $[k_{ET}]_{Blend} \propto R^{-6}$ and of bilayers $[k_{ET}]_{Bilayer} \propto R^{-2}$ to be comparable. Thus,

$$[[k_{ET}]_{Blend} \approx [k_{ET}]_{Bilayer} \implies R_{Bilayer} \propto (R_{Blend})^3. \quad (3)$$

By considering that $R_{Blend} \approx R_0 = 4.6$ nm, the estimated value for the distances [Eq. (3)] involved in the bilayers reaches $R_{Bilayer} \approx 97$ nm. This result strongly indicates that the energy transfer in bilayers is a consequence of the surface-surface interaction geometry, leading to larger donor/acceptor interaction distances, in agreement with the larger thickness of the layers in the bilayer structure. Further measurements, using a lithium-fluoride separation layer in between the donor and acceptor layers, where the thickness can be controlled, are being planned in order to have a complete understanding of the energy transfer mechanism in those bilayer structures.

IV. CONCLUSIONS

PFO/MEH PPV bilayers and PFO:MEH PPV blends were studied by steady-state photoluminescence, absorption, and time-resolved photoluminescence in the air at room temperature. Both systems enabled us to observe a relatively strong energy transfer effect from the PFO donors to the MEH PPV acceptors. The energy transfer performance in

these system has been estimated by the ratio between the MEH PPV peak intensities obtained by exciting the PFO donor sites directly at 373 nm, and by exciting just the MEH PPV acceptor sites at 488 nm. Those ratios together with the respective PLQY values enabled us to conclude that the energy transfer rates in both structures were comparable. This demonstrated that an effective and relatively high energy transfer in bilayers fabricated by a sequential spin-coating can be achieved. The decays acquired at 424 nm, corresponding to the decays of the PFO emission presented comparable shorter lifetimes, confirming the energy transfer effect in the the bilayer B1 and in the blends at 5.4% and 11.5% MEH PPV concentrations. The enhancement of the MEH PPV emission due to the energy transfer effect also enabled us to investigate the decay behaviors for the acceptor states and put aside the different characteristics of blends and bilayers.

In the blends, the dominant long lifetime terms take place for the MEH PPV acceptor decays and were related to the existence of exciplex transitions. The analysis of the PL intensity on temperature has shown that exciton migration (more likely at higher temperatures) and Förster energy transfer (dominant at lower temperatures) both contribute to the energy transfer from PFO to MEH PPV. In the blends, clear evidence of the exciplex states is also seen.

Conversely to the blends, the PL and PLE intensities in the bilayer monotonically increase with decreasing temperature. The decay of the acceptor emission in the bilayer presented an important contribution from the MEH PPV lifetime. This has enabled us to interpret the energy transfer as a consequence of a direct surface-surface interaction between PFO and MEH PPV, involving distances ($R_{\text{Bilayer}} \approx 97$ nm) much larger than the Förster radius, in agreement to what it was expected due to the thicker PFO layers in the bilayers.

ACKNOWLEDGMENTS

LAC thanks FAPEMIG, CAPES for financial support, and also CNPq from Brazil for the visitor fellowship during his sabbatical period at the Physics Department, University of Durham, United Kingdom.

¹S. A. Jenekhe, X. Zhang, X. L. Chen, V.-E. Choong, Y. Gao, and B. R. Hsieh, *Chem. Mater.* **9**, 409 (1997).

- ²N. C. Greenham, S. C. Moratti, D. D. C. Bradley, R. H. Friend, and A. B. Holmes, *Nature (London)* **365**, 628 (1993).
- ³S. Dailey, M. Halim, E. Rebourt, L. E. Horsburgh, I. D. W. Samuel, and A. P. Monkman, *J. Phys.: Condens. Matter* **10**, 5171 (1998).
- ⁴X. Zhang and S. A. Jenekhe, *Macromolecules* **33**, 2069 (2000).
- ⁵D. D. Gebler, Y. Z. Wang, J. W. Blatchford, S. W. Jessen, D. K. Fu, T. M. Swager, A. G. MacDiarmid, and A. J. Epstein, *Appl. Phys. Lett.* **70**, 1644 (1997).
- ⁶A. Huijser, T. J. Savenije, A. Shalav, and L. D. A. Siebbeles, *J. Appl. Phys.* **104**, 034505 (2008).
- ⁷J. C. de Mello, H. F. Wittmann, and R. H. Friend, *Adv. Mater.* **9**, 230 (1997).
- ⁸R. Zhu, J.-M. Lin, W.-Z. Wang, C. Zheng, W. Wei, W. Huang, Y.-H. Xu, J.-B. Peng, and Y. Cao, *J. Phys. Chem. B* **112**, 1611 (2008).
- ⁹L.-O. Palsson and A. P. Monkman, *Adv. Mater.* **14**, 757 (2002).
- ¹⁰F. B. Dias, M. Knaapila, A. P. Monkman, and H. D. Burrows, *Macromolecules* **39**, 1598 (2006).
- ¹¹L. Smilowitz, A. Hays, A. J. Heeger, G. Wang, and J. E. Bowers, *J. Chem. Phys.* **98**, 6504 (1993).
- ¹²M. Yan, L. J. Rothberg, E. W. Kwoke, and T. M. Miller, *Phys. Rev. Lett.* **75**, 1992 (1995).
- ¹³B. Ali, S. Jabar, W. Salih, R. K. Al Tamini, H. Al Attar, and A. P. Monkman, *Opt. Mater.* **32**, 350 (2009).
- ¹⁴S.-An Chen, H.-Hung Lu, and C.-Wei Huang, *Adv. Polym. Sci.* **212**, 49 (2008).
- ¹⁵A. L. Holt, J. M. Leger, and S. A. Carter, *J. Chem. Phys.* **123**, 044704 (2005).
- ¹⁶A. Rose, J. D. Tovar, S. Yamaguchi, E. E. Nesterov, Z. Zhu, and T. M. Swager, *Philos. Trans. R. Soc. London, A* **365**, 1589 (2007).
- ¹⁷J. J. B.-Smith, J. Wilson, C. D.-Smith, K. Mouri, S. Yamaguchi, H. Murata, and J. Nelson, *J. Phys. Chem. B* **113**, 7794 (2009).
- ¹⁸F. B. Dias, K. T. Kamtekar, T. Cazati, G. Williams, M. R. Bryce, and A. P. Monkman, *ChemPhysChem* **10**, 2096 (2009).
- ¹⁹M. Ariu, M. Sims, M. D. Rahn, J. Hill, A. M. Fox, D. G. Lidzey, M. Oda, J. Cabanillas-Gonzalez, and D. D. C. Bradley, *J. Phys.: Condens. Matter* **67**, 195333 (2003).
- ²⁰M. J. Winokur, J. Slinker, and D. L. Huber, *J. Phys.: Condens. Matter* **67**, 184106 (2003).
- ²¹I. D. W. Samuel, G. Rumbles, C. J. Collison, R. H. Friend, S. C. Moratti, and A. B. Holmes, *Synth. Met.* **84**, 497 (1997).
- ²²J.-W. Yu, J. K. Kim, H. N. Cho, D. Y. Kim, C. Y. Kim, N. W. Song, and D. Kim, *Macromolecules* **33**, 5443 (2000).
- ²³P. E. Shaw, A. Ruseckas, and I. D. W. Samuel, *Phys. Rev. B* **78**, 245201 (2008).
- ²⁴Joseph R. Lakowicz, *Principles of Fluorescence Spectroscopy*, 2nd. ed. (Kluwer Academic/Plenum, New York, 1999), p. 369.
- ²⁵P. N. Stravinou, G. Ryu, M. Campoy-Quiles, and D. D. C. Bradley, *J. Phys.: Condens. Matter* **19**, 466107 (2007).
- ²⁶S. Masuo, T. Tanaka, S. Machida, and A. Itaya, *Appl. Phys. Lett.* **92**, 233114 (2008).
- ²⁷J. Cabanillas-Gonzalez, A. M. Fox, J. Hill, and D. D. C. Bradley, *Chem. Mater.* **16**, 4705 (2004).
- ²⁸J. Hill, S. Y. Heriot, O. Worsfold, T. H. Richardson, A. M. Fox, and D. D. C. Bradley, *Synth. Met.* **139**, 787 (2003).
- ²⁹B. R. Postacchini, V. Zucolotto, F. B. Dias, A. Monkman, and O. N. Oliveira, Jr., *J. Phys. Chem. C* **113**, 10303 (2009).